AEROELASTIC CONTROL OF HELICOPTER BLADE SAILING IN UNSTEADY FLOW USING SMART MATERIALS

Vinícius Piccirillo, pcmec@ita.br
Kleber Augusto Lisboa Castão, kcastao@ita.br
Roberto Luiz da Cunha Barroso Ramos, rlcbramos@gmail.com
Luiz Carlos Sandoval Goes, goes@ita.br
Department of Engineering Aeronautical and Mechanical, Tecnological Institute of Aeronautics – ITA, 12228 – 900, Sao Jose dos Campos, SP, Brazil.

Abstract. *This paper analyzes the unsteady flow response of a helicopter blade-sailing control system using two different smart-materials strategies involving shape memory alloy (SMA) and magnetorheological damper (MRD). The aeroelastic analysis focuses on the performance of a proposed semi-active controller with respect to the reduction of blade flapping vibrations in articulated rotors during engagement shipboard operations. The designed control yields gust load alleviation by increasing the stiffness/damping of the flapping motion. The simulation results show that the proposed SMA/MR aeroelastic controller can yield tunnel-strike suppression and significant reduction in upward blade tip deflections at the unsteady wind-over-deck conditions of interest.*

Keywords*: Helicopter blade sailing, shape memory alloy, magnetorheological fluid, aeroelasticity, unsteady flow*

1. INTRODUCTION

Flow-induced unsteady loads are often related to large vibrations and damage in flexible structures. Shipboard helicopters, operating in the hostile maritime environment from frigate-like platforms, are especially susceptible to these effects during rotor engagement/disengagement operations under high wind-over-deck (WOD) conditions. These dangerous conditions are amplified by the ship structure, which generates flow velocity gradients and vortices over the flight deck. Therefore, shipboard helicopter operations are among the most hazardous military operations and the shipboard environment imposes severe restrictions on the missions and determines stringent requirements for the design of aerial vehicles.

The problem of flight in the vicinity of ships is usually called Dynamic Interface (DI) problem (Rhodes and Healey, 1992). Among the dynamic phenomena in the DI that must be analyzed and controlled, one is especially important for rotary-wing aircraft: *blade sailing*.

Blade sailing is an aeroelastic transient phenomenon characterized by the occurrence of large flapping vibrations, possibly associated with tunnel/tail-boom strikes, due to fluid-structure interactions during engagement or disengagement operations of helicopter rotors under high wind conditions (Newman, 1995). The blade-sailing control problem has a theoretical importance, due to the nonlinear time-varying characteristics of the associated blade flapping oscillator, which is also subjected to large disturbances. Considering the ubiquitous use of the shipboard helicopter in critical defense missions, the problem has a practical relevance as well, as shown by a recent NATO symposium about the study of flow-induced unsteady loads and the impact on military applications (Wall et al., 2005).

Semi-active aeroelastic control strategies, aimed at prescribing a low-vibration behavior for shipboard rotors in the DI by using smart-materials controllers, can enhance the survivability of shipboard helicopters and improve the safety of military operations in the hostile maritime environment. The increasing availability and low cost of electronic and smart-materials technology, including microcontrollers, sensors and actuators, stimulate semi-active control as a reliable substitute for passive control devices, such as dampers, mechanical pitch-flap couplings (δ_3) and spoilers. Previous research on blade-sailing control includes swashplate-actuation for gimballed rotors (Keller, 2001), use of trailing-edge flaps (Jones and Newman, 2007), active twist (Khouli et. al., 2008) and individual blade root control (Ramos, 2007; Ramos et al., 2009a, 2009b). The obtained theoretical results may be helpful for better understanding of helicopter blade-sailing alleviation using a shape memory alloy (SMA) element or a magnetorheological damper (MRD).

2. SMART-MATERIALS MODELING

2.1 SMA Constitutive Model

To describe the behavior of the shape memory alloy, the constitutive model proposed by Savi and Braga (1993) is adopted. This model is based on Devonshire theory and it defines a free energy of Helmholtz (ψ) in the polynomial form and it is capable to describe the shape memory and pseudoelasticity effects. The polynomial model is suitable for one-dimensional cases and it does not consider an explicit potential of dissipation, and no internal variable is considered. On this form, the free energy depends only on the observable state variables (temperature (T) and strain (ε)), that is, $\psi = \psi(\varepsilon, T)$.

The free energy is defined in such way that, for high temperatures ($T > T_A$), the energy has only one point of minimum corresponding to the null strain representing the stability of the austenite phase (A); for intermediate temperatures ($T_M < T < T_A$) it presents three points of minimum corresponding to the austenitic phase (A), and two martensitic phases (M^+ and M^-), which are induced by positive and negative stress fields, respectively; for low temperature ($T < T_M$), there are two points of minimum representing the two variants of martensite (M^+ and M^-), corresponding to the null strain.

Therefore, the above restrictions are given by the following polynomial equation:

$$\rho\psi(\varepsilon, T) = \frac{1}{2} q(T - T_M)\varepsilon^2 - \frac{1}{4} b\varepsilon^4 + \frac{1}{6} e\varepsilon^6 \quad , \tag{1}$$

where q and b are constants of the material, T_M corresponds to the temperature where the martensitic phase is stable, ρ is the SMA density, and the free energy has only one minimum at zero strain. The constant e may be expressed in terms of other constants of the material:

$$T_A = T_M + \frac{b^2}{4qe}, \tag{2}$$

where T_A corresponds to the temperature where the austenite phase is stable. Thus, the stress-strains relation is given by:

$$\sigma = q(T - T_M)\varepsilon - b\varepsilon^3 + \frac{b^2}{4q(T_A - T_M)}\varepsilon^5 \quad . \tag{3}$$

According to Paiva and Savi (2006), the polynomial model represents, in a qualitatively coherent way, both martensite detwinning process and pseudoelasticity, although it does not consider twinned martensite (M). In other words, there is no stable phase for $T < T_M$ in a stress-free state, but the authors believe that this analysis is useful to the understanding of the nonlinear dynamics of shape memory systems. The proposed model captures itself all of the essential features of the pseudoelasticity phenomenon for blade-sailing control.

2.2 MRD Modeling

It is well known that the magnetorheological fluid (MRF) consists of a mineral oil based fluid (or silicone, water, etc.) with micron magnetic particles in suspension, which line up in parallel to a applied magnetic field, forming a species of chain. When the structure is submitted to a vibration, these chains break, wasting energy and, the magnetic field cause the reconstruction of them. The continuous breaking and reconstitution of these chains allow the fluid to waste energy of the system (Lyu et al., 2000).

A simplified rheological model of a MRD is given by:

$$\zeta = \zeta_{y(field)} + \varsigma\dot{\varphi} \ , \tag{4}$$

where $\zeta_{y(field)}$ it is the yield stress induced of the magnetic field and ς is the fluid viscosity. A great number of authors have considered a mathematical model of MRD, known as Bingham model (Dyke et al., 1996; Stanway et al., 1985; Stanway et al., 1987). This model consists of two elements: an element modeled as being of the same type of Coulomb friction placed in parallel with a linear viscous damping element. Therefore, for velocities different of zero, the force generated by the device is given by:

$$F_B(i, \dot{x}) = f_d(i)\,\mathrm{sgn}(\dot{x}) + c_0(i)\dot{x}, \tag{5}$$

where, c_0 is the coefficient of viscous damping and f_d is the force related to the rheological behavior, linked to the strain that is produced by the fluid; both depend on the current (magnetic field) applied to the damper.

3. AEROELASTIC MODELING

For control purposes the blade-sailing aeroelastic model can be greatly simplified by considering the forces and moments actuating only in the flapping plane.

Fig. 1 shows the forces at a blade element for the simplified blade-sailing planar model, according to a frame rotating with the blade.

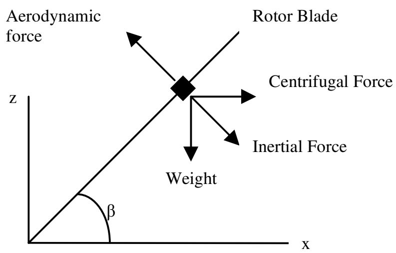

Figure 1: Forces at a flapping planar blade element for the proposed blade-sailing model (rotating frame)

The simplified diagram of forces at a planar blade element (Johnson, 1994) in Fig. 1 illustrates the main factors that govern the blade-sailing behavior. Ship motion effects are not included. The resulting moments about the flapping hinge in conjunction with the droop/flap stop effects, modeled as a nonlinear rotational spring, determine the blade tip deflections related to the angle β.

Fig. 2 shows the flow velocity components in the plane of the rotor for the proposed blade-sailing model, considering the WOD conditions. V_{WOD} and Ψ_{WOD} are, respectively, the magnitude and direction of the incoming wind velocity with respect to the ship centerline

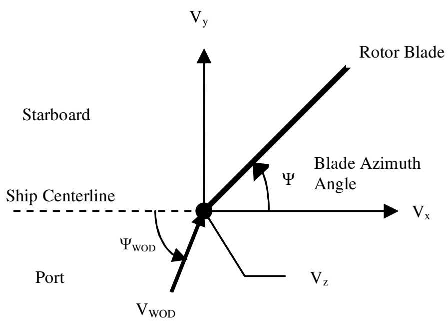

Figure 2: Flow velocity components for the WOD conditions

The blade-sailing modeling is based on a proposed rotary-wing aeroelastic scheme applied to articulated shipboard rotor blades, according to the Figs. 1 and 2, taking into account some simplifying assumptions (Ramos, 2007; Ramos et al., 2009a, 2009b).

According to the Newtonian approach for rotation, to the d'Alembert principle, to the diagram of forces in Fig. 1, and to the modeling assumptions, the sum of the total moments about the flapping hinge is given by:

$$M_i - M_{as} + M_c + M_s + M_g = 0\,, \tag{6}$$

where M_i is the moment due to the inertial forces, M_{as} is the moment due to the aerodynamic forces related to the ship airwake, collective/cyclic commands and rotor blade motions, M_c is the moment due to the centrifugal forces, M_s is the moment due to the droop and flap stops, and M_g is the moment due to the gravity effects.

The total moment due to the inertial forces at each blade element with mass dm at station r is given by:

$$M_i = \int_0^R r\,\ddot{\beta}\,dm\,r = I_B\ddot{\beta}\,, \tag{7}$$

where I_B is the blade moment of inertia about the center of rotation and β is the blade flapping angle.

The total moment due to the centrifugal forces at each blade element with mass *dm* at station *r* is given by:

$$M_c = \int_0^R r\sin\beta\,\Omega^2\, r\cos\beta\, dm = I_B\Omega^2 \sin\beta\cos\beta \approx I_B\Omega^2\beta, \tag{8}$$

where *R* is the rotor radius and *Ω*, the rotor rotational speed, is time-dependent during the engagement or disengagement rotor operations. The approximation for small flapping angles is applied.

Considering a uniform distribution of the blade mass μ, the total moment due to the acceleration of gravity *g* is:

$$M_g = \int_0^R \mu g\cos\beta r dr = \mu\frac{R^2}{2} g\cos\beta = I_B\frac{3}{2R} g\cos\beta \approx I_B\frac{3}{2R} g. \tag{9}$$

Articulated rotors usually have droop and flap stops, located near the blade roots, aimed at restricting the downward and upward flapping deflections, respectively, during low rotational speeds. During hover and forward flight regimes, the stops remain deactivated.

To model the blade structural dynamics, it is assumed a flexible rotating blade, whose flapping motion about a hinge located near the root is restricted by droop and flap stops. A simplified model for the flexible blade dynamics can be obtained by considering the flapping motion as constituted by a rigid mode between the stops and cantilevered modes beyond the stop angles (Keller, 2001). The stop effects can be captured in a form suitable for the control design and analysis by considering a single nonlinear rotational spring, whose stiffness is negligible between the stops, where the articulated blade behaves as a rigid beam, and much increased beyond the stop angles, where the articulated blade behaves as a cantilever beam, affected by the non-rotating blade flexibility properties, which are associated with the flapwise bending stiffness and the natural frequencies. Figs. 3 and 4 illustrate the blade deflections during droop stop contacts (Keller, 2001) and the nonlinear rotational spring approximation (Ramos, 2007; Ramos et al., 2009a, 2009b), respectively.

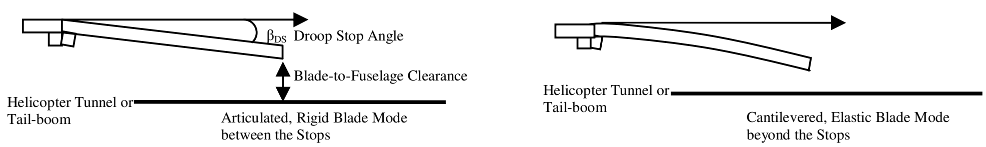

Figure 3: Blade deflections during droop stop contacts

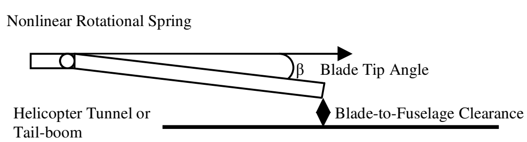

Figure 4: Nonlinear rotational spring approximation of the droop/flap stop effects

The spring constant K_β can be obtained from a simplified model for a flexible, hingeless blade, with Southwell coefficient approximately 1 and rotating flapping natural frequency ω_r given by Dowell (1995):

$$\omega_r^2 \approx \frac{K_\beta}{I_B} + \Omega^2 = \omega_{nr}^2 + \Omega^2, \tag{10}$$

where ω_{nr} is the blade non-rotating flapping natural frequency.

According to Eq. 10, the parameter K_β, related to the cantilevered mode of the blade behavior beyond the stops, is given by:

$$K_\beta = I_B\omega_{nr}^2, \tag{11}$$

where

$$\omega_{nr}^2 = k\frac{EI_{yy}}{\mu R^4}. \tag{12}$$

In Eq. 12, k is a constant related to the cantilevered, elastic blade behavior. Therefore, the nonlinear spring moment due to the stops, can be modeled as:

$$\mathrm{M_s} = \mathrm{I_B}\sigma_1(\beta)\,, \tag{13}$$

where the function $\sigma_1(\beta)$ is given by:

$$\begin{aligned} &\sigma_1(\beta) = \omega_{nr}^2(\beta - \beta_{FS}), \text{if } \beta > \beta_{FS} \\ &\sigma_1(\beta) = 0, \text{if } \beta_{DS} \le \beta \le \beta_{FS} \\ &\sigma_1(\beta) = \omega_{nr}^2(\beta - \beta_{DS}), \text{if } \beta < \beta_{DS} \end{aligned} \tag{14}$$

where β_{DS} and β_{FS} are, respectively, the droop and flap stop angles. From Eqs. 6, 7, 8, 9, and 13 the articulated-rotor blade-sailing dynamics is given by:

$$\mathrm{I_B}\ddot{\beta} + \mathrm{I_B}\Omega^2\beta + \mathrm{I_B}\sigma_1(\beta) = -\mathrm{I_B}\frac{3}{2\mathrm{R}}\mathrm{g} + \mathrm{M_{as}}\,. \tag{15}$$

The three-dimensional ship airwake pattern can be modeled according to the mean ($\overline{V_x}, \overline{V_y}, \overline{V_z}$) and fluctuating ($V_x', V_y', V_z'$) flow velocity WOD components, as follows (Keller, 2001):

$$\mathrm{V_x} = \overline{\mathrm{V_x}} + \mathrm{V_x}, \quad \mathrm{V_y} = \overline{\mathrm{V_y}} + \mathrm{V_y}, \quad \mathrm{V_z} = \overline{\mathrm{V_z}} + \mathrm{V_z}\,. \tag{16}$$

Generally, the flow field that affects the rotor behavior is non-uniform and unsteady, thus, the three velocity components vary with space and time. Mean flow velocity gradients arise due to the ship geometry and the fluctuating flow velocity components arise due to the ship geometry and also to the meteorological effects, like turbulence from storms.

To simplify the aeroelastic analysis, only the lateral (90^o or 270^o) wind condition is considered, focusing the ship airwake modeling on the effects of the horizontal and vertical velocity components related to this worst-case blade-sailing condition (Newman, 1995). The WOD velocity component V_x is neglected. For a typical frigate-like configuration with only one flight deck, as considered in this work, the WOD horizontal velocity V_y for the lateral condition can be considered uniform along the shipboard rotor.

The mean flow vertical velocity related to the interaction between the lateral undisturbed wind flow and a typical frigate-like structure can be approximated by a linear distribution along the flight deck and the helicopter rotor (Geyer et. al., 1998; Newman, 1990). Therefore, for a rotor blade element at radial station r and azimuth Ψ, and constant WOD horizontal velocity component V_y, the WOD mean vertical velocity, according to the linear distribution approximation ("linear gust model"), is given by:

$$\overline{V_z} = K_v V_y \frac{r}{R}\sin\Psi\,. \tag{17}$$

Unsteady flow effects can be modeled by considering a sinusoidal gust across the rotor disk for the WOD fluctuating vertical velocity component, representing the effects of the dominant frequency ω_f of the ship airwake on the helicopter rotor, as follows:

$$V_z' = K_f V_y \sin\omega_f t\,. \tag{18}$$

The gust amplitude parameters K_v and K_f, and the sinusoidal gust frequency ω_f govern the flow-induced unsteady loads associated with the WOD vertical velocity component, which characterizes a flow field over the flight deck that varies with space and time according to Eqs. 17 and 18.

The aerodynamic components affecting a shipboard rotor blade can be calculated according to the blade-element theory, as follows (Keller, 2001):

$$\begin{aligned} &\mathrm{V_x} = \mathrm{V_{WOD}}\cos\Psi_{\mathrm{WOD}}, \quad \mathrm{V_y} = \mathrm{V_{WOD}}\sin\Psi_{\mathrm{WOD}}, \\ &\mathrm{U_T} = \Omega \mathrm{r} - \mathrm{V_y}\cos\Psi + \mathrm{V_x}\sin\Psi, \quad \mathrm{U_P} = \mathrm{r}\dot{\beta} + (\mathrm{V_y}\sin\Psi + \mathrm{V_x}\cos\Psi)\beta - \mathrm{V_z}\,. \end{aligned} \tag{19}$$

In particular, Ψ_{WOD} is equal to 90° for lateral port side winds and to 270° for lateral starboard side winds. U_P and U_T are, respectively, the normal and tangential flow velocity components at the blade element at radial station r, azimuth Ψ and flapping angle β. These flow velocity components are illustrated in Fig. 5, according to the blade-element theory (Dowell et. al., 1995). $V_z(r,\Psi)$ is the WOD vertical velocity at a blade element and $\Omega(t)$ is the time-varying rotational speed during shipboard engagement or disengagement operations.

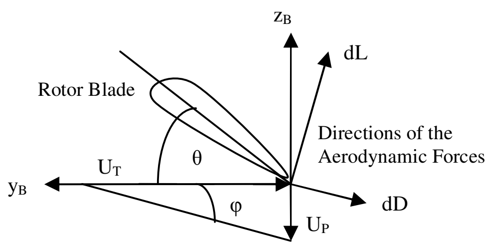

Figure 5: Aerodynamic forces and flow velocities at a blade element

The lift force dL and the aerodynamic moment dM_{as} for a blade element can be obtained from the equations:

$$\begin{aligned} &\theta_0 = \theta_{.75} - (3/4)\theta_{tw}, \quad \theta = \theta_0 + \theta_{1s}\sin\Psi + \theta_{1c}\cos\Psi + \theta_{tw}(r/R) \\ &\alpha = \theta - (U_P/U_T), \quad dL = (1/2)\rho U_T^2 c a \alpha\, dr, \quad dM_{as} = r\, dL \end{aligned}, \tag{20}$$

Eq. 20 yields the following aerodynamic moment at a blade element on the radial position r:

$$dM_{as} = \frac{1}{2}\rho U_T^2 ca\left(\theta - \frac{U_P}{U_T}\right) rdr = \frac{1}{2}\rho ac\left(\theta U_T^2 - U_P U_T\right) rdr \,. \tag{21}$$

Substituting the expressions for the blade-element flow velocities given by Eq. 20 into Eq. 21 and integrating along the blade, yields:

$$M_{as} = \frac{1}{2}\rho ac\int_0^R \left\{\theta\left(\Omega r - V_y\cos\Psi + V_x\sin\Psi\right)^2 - \left(\Omega r - V_y\cos\Psi + V_x\sin\Psi\right)\left[r\dot{\beta} + (V_y\sin\Psi + V_x\cos\Psi)\beta - V_z\right]\right\} rdr \tag{22}$$

Considering that:

$$I_B = \frac{\mu R^3}{3}; \quad \gamma \equiv \frac{3\rho acR}{\mu}; \quad \mu_x \equiv \frac{V_x}{\Omega R}; \quad \mu_y \equiv \frac{V_y}{\Omega R}, \tag{23}$$

where γ is the Lock number and μ_x, μ_y are advance ratio parameters, Eq. 22 yields for the blade aerodynamic moment:

$$M_{as} = M_{ai} + M_{atw} + M_{a\dot{\beta}} + M_{a\beta} + M_{az}, \tag{24}$$

where:

$$\begin{aligned} &M_{ai} = I_B\frac{\gamma\Omega^2}{8}\left[1 + \frac{8}{3}\left(\mu_x\sin\Psi - \mu_y\cos\Psi\right) + 2\left(\mu_x\sin\Psi - \mu_y\cos\Psi\right)^2\right]\theta_i, \quad M_{atw} = I_B\frac{\gamma\Omega^2}{2}\left[\frac{1}{5} + \frac{1}{2}\left(\mu_x\sin\Psi - \mu_y\cos\Psi\right) + \frac{1}{3}\left(\mu_x\sin\Psi - \mu_y\cos\Psi\right)^2\right]\theta_{tw} \\ &M_{a\dot{\beta}} = I_B\frac{\gamma\Omega}{8}\left[-1 - \frac{4}{3}\left(\mu_x\sin\Psi - \mu_y\cos\Psi\right)\right]\dot{\beta}, \quad M_{a\beta} = I_B\frac{\gamma\Omega^2}{8}\left[-\frac{4}{3}\left(\mu_x\cos\Psi + \mu_y\sin\Psi\right) + \left(\mu_y^2 - \mu_x^2\right)\sin 2\Psi + 2\mu_x\mu_y\cos 2\Psi\right]\beta \\ &M_{az} = I_B\frac{\gamma\Omega}{8R}\left\{\left[1 + \frac{4}{3}\left(\mu_x\sin\Psi - \mu_y\cos\Psi\right)\right]V_{zg} + \left[\frac{4}{3} + 2\left(\mu_x\sin\Psi - \mu_y\cos\Psi\right)\right]V_{zu}\right\} \end{aligned} \tag{25}$$

and

$$\theta_i = \theta_0 + \theta_{1s}\sin\Psi + \theta_{1c}\cos\Psi, \quad V_{zg} = K_v V_y \sin\Psi, \quad V_{zu} = K_f V_y \sin\omega_f t \tag{26}$$

In Eq. 24, $M_{ai}, M_{atw}, M_{a\dot{\beta}}, M_{a\beta}, M_{az}$ are, respectively, the aerodynamic moments due to the blade pitch input, to the blade built-in twist, to the blade flapping rate, to the blade flapping angle, and to the WOD vertical velocity. The WOD vertical velocity factor related to the flow velocity gradients V_{zg} in Eq. 25 is valid, in particular, for lateral wind conditions (V_x = 0, Ψ_{WOD} = 90° or 270°), according to the linear distribution approximation for the ship airwake given by Eq. 17.

The adopted rotational speed profile is based on the shipboard rotor engagement characteristics of the H-46 Sea Knight helicopter (Keller, 2001).

The aerodynamic moments associated with the flapping angle and rate in Eq. 25 introduce time-varying coefficients on the blade flapping motion/blade-sailing equation.

Smart materials can be applied to the reduction of blade-sailing vibrations by means of flapping stiffness/damping effects. As mentioned in the introduction, previous researches on blade-sailing active control were based on swashplate actuation (Keller, 2001), trailing edge flaps (Jones and Newman, 2007), active twist (Khouli et. al., 2008) and individual blade root control (Ramos, 2007; Ramos et al., 2009a, 2009b).

Substituting Eqs. 24 and 25 into Eq. 15, dividing by I_B, and introducing the smart-materials stiffness/damping effects:

$$\begin{aligned}
&\ddot{\beta}+\frac{\gamma\Omega}{8}\left[1+\frac{4}{3}\left(\mu_x \sin\Psi-\mu_y\cos\Psi\right)\right]\dot{\beta}+\Omega^2\left\{1+\frac{\gamma}{8}\left[\frac{4}{3}\left(\mu_x\cos\Psi+\mu_y\sin\Psi\right)-\left(\mu_y^2-\mu_x^2\right)\sin 2\Psi-2\mu_x\mu_y\cos 2\Psi\right]\right\}\beta+\sigma_1(\beta)+K_{SMA}(\beta,T)= \\
&\frac{\gamma\Omega^2}{8}\left[1+\frac{8}{3}\left(\mu_x\sin\Psi-\mu_y\cos\Psi\right)+2\left(\mu_x\sin\Psi-\mu_y\cos\Psi\right)^2\right]\theta_u+\frac{\gamma\Omega^2}{8}\left[1+\frac{8}{3}\left(\mu_x\sin\Psi-\mu_y\cos\Psi\right)+2\left(\mu_x\sin\Psi-\mu_y\cos\Psi\right)^2\right]\theta_i+ \\
&\frac{\gamma\Omega^2}{2}\left[\frac{1}{5}+\frac{1}{2}\left(\mu_x\sin\Psi-\mu_y\cos\Psi\right)+\frac{1}{3}\left(\mu_x\sin\Psi-\mu_y\cos\Psi\right)^2\right]\theta_{tw} \\
&+\frac{\gamma\Omega}{8R}\left\{\left[1+\frac{4}{3}\left(\mu_x\sin\Psi-\mu_y\cos\Psi\right)\right]V_{zg}+\left[\frac{4}{3}+2\left(\mu_x\sin\Psi-\mu_y\cos\Psi\right)\right]V_{zu}\right\}-\frac{3}{2R}g
\end{aligned} \tag{27}$$

$$\begin{aligned}
&\ddot{\beta}+\frac{\gamma\Omega}{8}\left[1+\frac{4}{3}\left(\mu_x \sin\Psi-\mu_y\cos\Psi\right)\right]\dot{\beta}+\Omega^2\left\{1+\frac{\gamma}{8}\left[\frac{4}{3}\left(\mu_x\cos\Psi+\mu_y\sin\Psi\right)-\left(\mu_y^2-\mu_x^2\right)\sin 2\Psi-2\mu_x\mu_y\cos 2\Psi\right]\right\}\beta+\sigma_1(\beta)+F_B(i,\dot{\beta})= \\
&\frac{\gamma\Omega^2}{8}\left[1+\frac{8}{3}\left(\mu_x\sin\Psi-\mu_y\cos\Psi\right)+2\left(\mu_x\sin\Psi-\mu_y\cos\Psi\right)^2\right]\theta_u+\frac{\gamma\Omega^2}{8}\left[1+\frac{8}{3}\left(\mu_x\sin\Psi-\mu_y\cos\Psi\right)+2\left(\mu_x\sin\Psi-\mu_y\cos\Psi\right)^2\right]\theta_i+ \\
&\frac{\gamma\Omega^2}{2}\left[\frac{1}{5}+\frac{1}{2}\left(\mu_x\sin\Psi-\mu_y\cos\Psi\right)+\frac{1}{3}\left(\mu_x\sin\Psi-\mu_y\cos\Psi\right)^2\right]\theta_{tw} \\
&+\frac{\gamma\Omega}{8R}\left\{\left[1+\frac{4}{3}\left(\mu_x\sin\Psi-\mu_y\cos\Psi\right)\right]V_{zg}+\left[\frac{4}{3}+2\left(\mu_x\sin\Psi-\mu_y\cos\Psi\right)\right]V_{zu}\right\}-\frac{3}{2R}g
\end{aligned} \tag{28}$$

Note, in Eq. (27), that the restitution force may be expressed as $K_{SMA} = \sigma A$, where A is the area of the SMA element, which is placed at the blade root. The MRD is placed between the rotor mast and the helicopter blade, in order to increase the damping of the flapping motion. In Eq. (28), the Bingham model of MRD is applied.

4. MODEL VERIFICATION AND NUMERICAL SIMULATION

The verification of the blade-sailing model given by Eqs. 27 and 28 is obtained by comparison with results given in (Keller, 2001; Geyer et. al., 1998) from models validated with experimental data, according to a fourth-fifth order Runge-Kutta numerical simulation. Table 1 shows the parameter values for the simulations, which are based on the H-46 Sea Knight shipboard helicopter characteristics, in conjunction with a WOD linear gust parameter K_v equal to 0.25.

Table 1: Parameters for the model verification

γ (Lock number)	7.96
Ω_0 (nominal rotor rotational speed)	27.65 rad/s
V_y (lateral WOD velocity)	- 42.5 kt
V_x (longitudinal WOD velocity)	0 kt
R (rotor radius)	25.5 ft
ω_{nr} (blade non-rotating flapping frequency)	6 rad/s
β_{DS} (droop stop angle)	- 1°
B_{FS} (flap stop angle)	1°
$\theta_{.75}$ (collective pitch angle)	3°
θ_{tw} (built-in twist angle)	- 8.5°
θ_{1s} (longitudinal cyclic angle)	2.5°
θ_{1c} (lateral cyclic angle)	0.0693°

A numerical simulation is carried out for the linear gust model of the ship airwake and Fig. 6 illustrates the results.

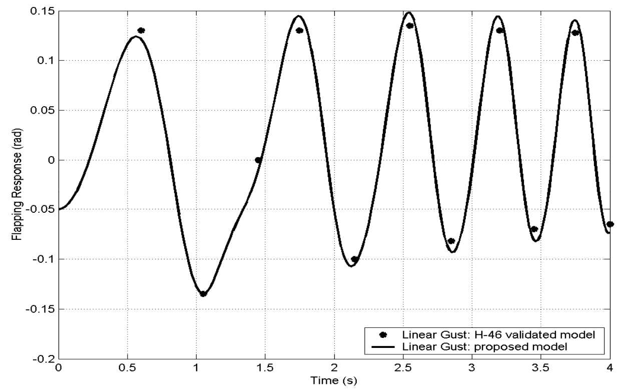

Figure 6: Flapping response for the linear gust model

The flapping response diagram in Fig. 6 shows a very good agreement of the proposed model with the results given in (Geyer e.tal., 1998). The time range 0-4 seconds of the simulation corresponds to 6-10 seconds for the actual H-46 engagement behavior, when rotor rotational speeds are low, varying from 10% to 46% of the nominal rotation speed (NR).

As the shape memory alloy presents different properties, depending on the temperature, a study on the pseudoelastic dynamic behavior is presented, considering a higher temperature, where austenitic phase is stable in the alloy. In all simulations, in order to analyze the behavior of the aeroelastic dynamical system, the spring is assumed to be made of a Ni-Ti alloy and the properties are presented in Table 2 (Paiva and Savi, 2006). In this case, it is used a temperature of the alloy around $T = 315K$ (approximately $T \approx 42°C$), and it is assumed a SMA element with $\mathrm{A} = 10^{-5}\,\mathrm{m}^2$.

Table 2. Material constants for a Ni-Ti alloy

Parameter	Units	Values
q	MPa/K	1000
b	Mpa	40×10^6
T_M	K	287
T_A	K	313

The performance of a blade-sailing controller using a SMA spring is then analyzed considering unsteady flow effects. Fig 7 shows the flapping response of the system for a sinusoidal gust with amplitude equal to 10% of the incoming flow velocity and frequency range of 4 to 6 rad/s. These simulation conditions correspond to measured unsteady flow characteristics over a typical ship's flight deck (Keller, 2001). Fig. 8 shows the effect of the nonlinear MRD on the blade flapping response, for the same gust conditions that are used in the SMA simulations. The applied current to the damper is i = 0.25A. With this value of current, a significant MRD effect on the blade-sailing phenomenon can be observed. It is obtained a reduction of approximately 30% in the flapping vibrations for both the SMA and MRD elements. Therefore, it is possible to avoid tunnel strikes by using these smart-material devices.

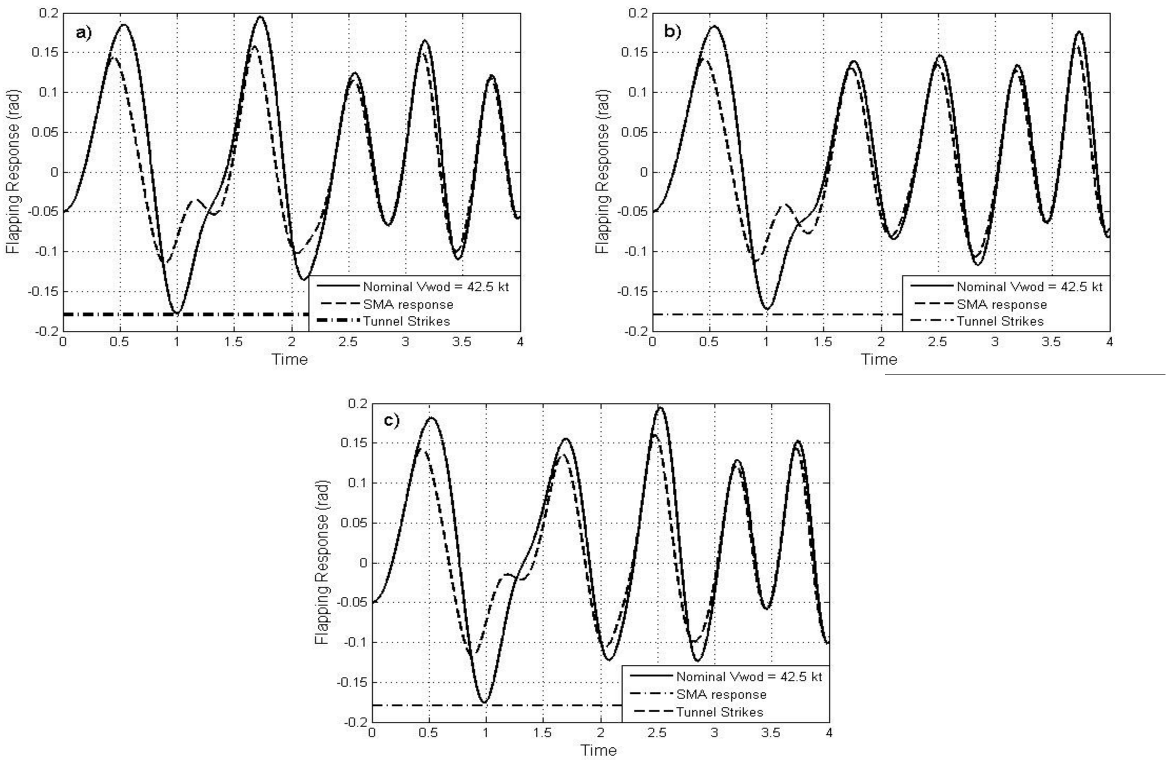

Figure 7: SMA response: (a) $K_f = 0.1$ and $\omega_f = 5$ rad/s, (b) $K_f = 0.1$ and $\omega_f = 4$ rad/s, (c) $K_f = 0.1$ and $\omega_f = 6$ rad/s

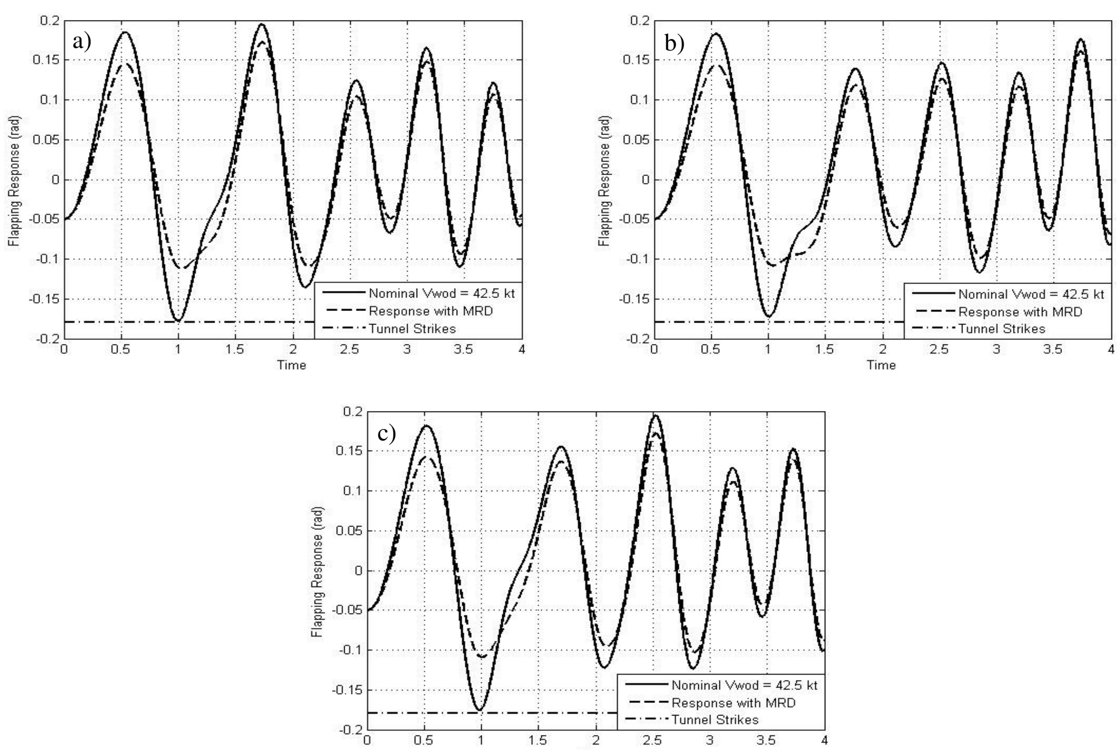

Figure 8: Response with MRD: (a) $K_f = 0.1$ and $\omega_f = 5$ rad/s, (b) $K_f = 0.1$ and $\omega_f = 4$ rad/s, (c) $K_f = 0.1$ and $\omega_f = 6$ rad/s

5. CONCLUSION

This paper analyzed the influence of smart-materials controllers on the helicopter blade-sailing phenomenon. A study on the pseudoelastic behavior of a SMA element was presented, considering a higher temperature, where austenitic phase is stable in the alloy. The simulations showed that a temperature-controlled SMA element can compensate high lift conditions during engagement shipboard operations by modifying the stiffness properties of the flapping oscillator. The effects of flapping damping enhancement by using a MRD element were modeled and simulated as well. The simulation results showed that a MRD device can significantly reduce the blade-sailing vibrations, avoiding tunnel-strike occurrences at severe unsteady flow conditions.

6. ACKNOWLEDGEMENTS

The authors thank the support of the Brazilian government Agency CNPq and Capes.

7. REFERENCES

Dowell, E.H. et al. (ed.). A Modern Course in Aeroelasticity. Kluwer Academic, 1995. Chapter 7. p. 370-437.

Dyke, S. J., Spencer, B. F., Sain, M. K., Carlson, J. D., 1996, Phenomenological model of a Magneto-rheological damper. ACSE Journal of Engineering Mechanics.

Geyer JR., W.P., Smith, E.C., Keller, J.A., 1998, “Aeroelastic Analysis of Transient Blade Dynamics During Shipboard Engage/Disengage Operations”. Journal of Aircraft, v. 35, n. 3, p. 445-453.

Haber, A., Jacklin, S.A., DeSimone, G., 2002, “Development, Manufacturing, and Component Testing of An Individual Blade Control System For a UH-60 Helicopter Rotor”. In: American Helicopter Society Aerodynamics, Acoustics, and Test and Evaluation Technical Specialists Meeting, San Francisco, CA.

Jones, M.P., Newman, S.J., 2007, “A Method of Reducing Blade Sailing through the Use of Trailing Edge Flaps”. In: American Helicopter Society Annual Forum, 63.

Johnson, W. Helicopter Theory. [S.l.]: Dover, 1994, p. 1-767.

Keller, J.A., 2001, “Analysis and control of the transient aeroelastic response of rotors during shipboard engagement and disengagement operations”. Thesis (PhD) - The Pennsylvania State University.

Khouli, F., Wall, A.S., Langlois, R.G., Afagh F.F., 2008, “Investigation of the Feasibility of a Proposed Hybrid Passive and Active Control Strategy for the Transient Aeroelastic Response of Helicopter Rotor Blades During Shipboard Engage and Disengage Operations”. In: American Helicopter Society Annual Forum, 64.

Liu Y., Gordaninejad F. ; Evrensel C. A. ; Wang X., Hitchock A, 2000, Semi active Control of A Bridge Using Controllable Magneto-Rheological Dampers, Proceedings of SPIE Conference on Smart Materials and Structures, Newport Beach, California.

Newman, S.J., 1995, “The Verification of a Theoretical Helicopter Rotor Blade Sailing Method by Means of Windtunnel Testing”. The Aeronautical Journal of the Royal Aeronautical Society, v. 99, n. 982, p. 41-51.

Newman, S.J., 1990, “A Theoretical Model for Predicting the Blade Sailing Behaviour of a Semi-Rigid Rotor Helicopter”. Vertica, 14, (4), p. 531-544.

Paiva, A., Savi, M.A., 2006, “An Overview of Constitutive Models for Shape Memory Alloy”, Mathematical Problem in Engineering, Vol. 2006, pp. 1 – 30.

Ramos, R. L. C. B., 2007, “Aeroservoelastic Analysis of the Blade-Sailing Phenomenon in the Helicopter-Ship Dynamic Interface”. Thesis (D.Sc.) – Technological Institute of Aeronautics, Brazil.

Ramos, R.L.C.B., de Andrade, D., Goes, L.C.S., 2009a, “Individual Blade Root Control of Helicopter Blade Sailing for Articulated Shipboard Rotors”, 65th American Helicopter Society Annual Forum.

Ramos, R.L.C.B., de Andrade, D., Goes, L.C.S., 2009b, Aeroservoelastic Analysis of a Proposed Helicopter Blade-Sailing Feedback Control System in Unsteady Flow, 8th Brazilian Conference on Dynamics, Control and Applications, Bauru, May 18-22.

Rhoades, M.M., Healey, J.V., 1992, “Flight deck aerodynamics of a nonaviation ship”. Journal of Aircraft, v. 29, n. 4, p. 619-626, Jul.-Aug.

Savi, M., and Braga, A.M.B., 1993, “Chaotic Vibrations of an Oscillator with Shape Memory”, Journal of the Brazilian Society of Mechanical Sciences and Engineering, Vol. XV, pp. 1 – 20.

Wall, A.S., Zan, S.J, Langlois, R.G., Afagh F.F., 2005, “A Numerical Model for Studying Helicopter Blade Sailing in an Unsteady Airwake”. In: Flow-Induced Unsteady Loads and the Impact on Military Applications – NATO symposium.

8. RESPONSIBILITY NOTICE

The authors are the only responsible for the printed material included in this paper.